Multiphysics Simulation Of 2nd Generation ^{238}Pu Production Designs Using COMSOL®

C. J. Hurt[1*], J. D. Freels[1†], A. Elzawawy[2]
1. Research Reactors Division, Oak Ridge National Laboratory, Oak Ridge, TN, USA
2. Vaughn College of Aeronautics and Technology, East Elmhurst, NY, USA
* Corresponding author, hurtcj@ornl.gov † Retired

1. Introduction

^{238}Pu is the principal radioisotope used as a power source for NASA deep space missions and space exploration vehicles. Target fabrication, irradiation, and chemical processing at Oak Ridge National Laboratory (ORNL) serves a critical function in re-establishing the domestic supply of ^{238}Pu.

In order to qualify experiments for in-vessel irradiation at the High Flux Isotope Reactor (HFIR) at ORNL, safety assessments need to be completed and documented to ensure adequate target cooling and structural integrity. Previously [1]-[2], finite element analysis tools in COMSOL Multiphysics ® [3] have been used to simulate steady state thermal-structural phenomena for targets containing neptunium dioxide in aluminum pellets (NpO2/Al) and their irradiation over three HFIR operating cycles to produce ^{238}Pu.

The production designs assessed previously have been updated, including both the target pin and the seven-pin target holder, to a "2nd Generation" design. The unique design of the new target holder requires new simulation physics and methodologies to act both as a design-aid tool and to re-assess individual target pin safety margin with regard to target cooling.

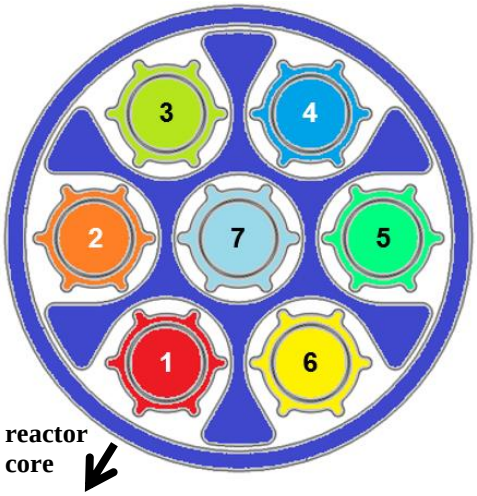

Figure 1. X-Y cross section at horizontal midplane of target holder extrusion with seven target pins.

1.1 2nd Generation Design

The 2nd Generation design [4] is an update to include improvements [5] to the previous ^{238}Pu production target and target holder. A significant design change with respect to the safety assessment is the change from concentric flow channels to non-symmetric channels for the six peripheral target pins, as shown in Fig. 1. Fig. 1 shows the seven target pins (where the reactor core is radially inward of pin 1), the target holder sleeve, and "spider" extrusion that contains the target pins within their respective flow channels. Changes in the upper target holder for handling require the majority of flow to enter from side inlets. As a result, center target pin flow is introduced later via connecting "slots" in the spider extrusion.

1.2 Experiment Safety Review

The experiment safety review to qualify irradiation at the HFIR includes an initial neutron transport analysis [6], to provide heat generation rates, in part. This is followed by thermal analyses for both steady-state and accident transient conditions to ensure adequate target cooling and structural integrity (Fig. 2). Previously, COMSOL was used for steady-state analysis, however it is for this design extended to address transient conditions, as well.

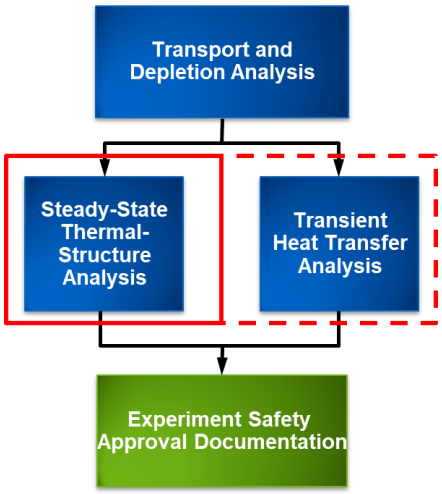

Figure 2. HFIR experiment safety review.

2. Use of COMSOL Multiphysics

COMSOL [3] version 5.3a is utilized for preliminary calculations and version 5.2 for the final simulations described herein. The modelling methodology required multiple simulation models in order to achieve the required safety envelope, as summarized in Fig. 3.

Physics interfaces used include: turbulent flow, heat transfer in liquids (and solids), solid mechanics, and non-isothermal pipe flow which utilize the CFD, Heat Transfer, Structural Mechanics, and Pipe Flow modules, respectively. In the thermal hydraulic models, the CAD Import Module is used to import the 2nd Generation target pin and target holder geometries, and the Design Module is used to repair and remove features. Built-in material properties or those developed previously [7] are used, with good comparison between built-in water properties and NIST[8].

Three sets of models utilized were the (1) CFD models of the target holder flow, (2) Thermal-structural models of the target pin, and (3) Pipe flow model for transient analysis. The first model is used for design-aid, experiment test validation[4], and safety analysis by computing steady-state overpower burnout margin as well as parameters (bulk temperature, heat transfer coefficients) for input into the latter two safety analysis models.

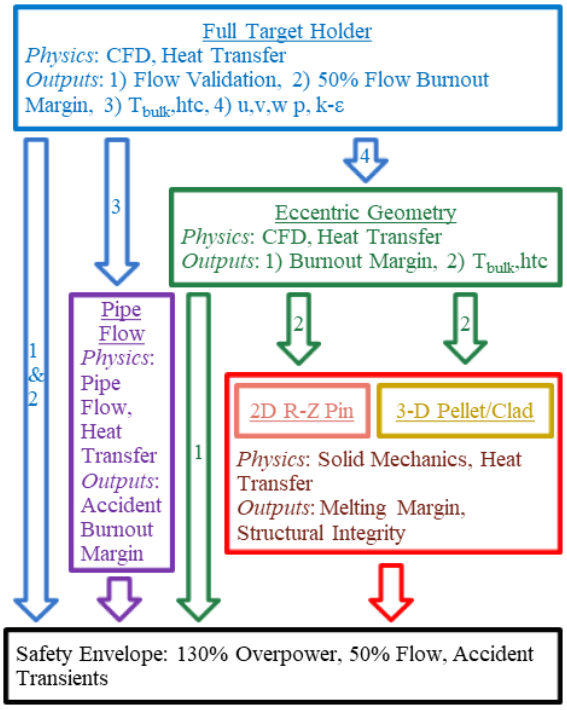

Figure 3. Modelling overview.

2.1 Thermal-Hydraulic Models

Two 3-D geometric model domains are considered for the CFD simulations: one sector of the entire holder length and another fully revolved geometry restricted to the finned axial length of the target pin. Both use the built-in k-ε turbulence model as the primary CFD physics, with the k-Ω turbulence model used as an alternate solution.

There are two geometric iterations of the full target holder model: a "flow test" geometry is used as both design-aid and for validation against flow test results, while a "design" geometry uses the as-built design for the safety assessment. The truncated fully revolved geometry is referred to as the eccentric geometry as it is used to study the effect of eccentric positions of target pins within their holder flow channels.

2.1.1 General Extrusion Operators

A special boundary condition is used in both thermal hydraulic models to transpose symmetric inlet/outlet conditions flow parameters onto slice or axially truncated x-y surfaces. General extrusion operators, a built-in COMSOL operator, are used to transpose and mirror the solution of 30 degree slices to identical x-y cross sections.

The source and destination frames have an identical radius (Eq. 1), while the destination angle is defined as a mirror of the source (Eq. 2). The destination frame x coordinate, x_d, can then be solved for by substitution of Eq. 2 into Eq. 1, and Eq. 1 is then solved for y_d, as shown in Eq. 3. These extrusions are duplicated, with adjustments to signs, to solve for the entire 360 degree rotation in the eccentric geometry outlets/inlets.

$$r_s = \sqrt{{x_s}^2 + {y_s}^2} = \sqrt{{x_d}^2 + {y_d}^2} = r_d \quad \textbf{(1)}$$

$$\theta_s = \operatorname{atan}\left(\frac{y_s}{x_s}\right);\ \theta_d = \frac{\pi}{3} - \theta_s = \operatorname{atan}\left(\frac{y_d}{x_d}\right) \quad \textbf{(2)}$$

$$x_d = \frac{r_d}{\sqrt{1+\tan^2\theta_d}};\ y_d = \sqrt{r_d^2 - {x_{dR}}^2} \quad \textbf{(3)}$$

2.1.2 Parameter Post-Processing

In order to extract flow parameters like bulk temperature, as shown in Fig. 3, an approach using the parametric sweep tool is used. First a parametric sweep is performed on an "empty" study that stores the final simulation results from the previous study step. Subsequently a volume average node is created under derived values, with an expression using logical expressions to restrict the integrated volume to a differential volume around a swept parameter. This is illustrated for a parameter sweep of axial position, z_p, in Eq. 4, for an expression of unity.

$$\frac{\iiint_V 1*\left[z' \le \left(z_{pi}+\frac{\Delta z}{2}\right)\right]*\left[z' \ge (z_{pi}-\frac{\Delta z}{2})\right]dV'}{\iiint_V dV'} = \frac{\iiint_{z_{pi}-\Delta z/2}^{z_{pi}+\Delta z/2} dx'dy'dz'}{\iiint_V dx'dy'dz'} = \frac{dV_i}{V_{channel}} \quad \textbf{(4)}$$

Since the denominator is not affected by the logical expression, however, the integrated numerator is divided by the total volume and the result for an expression of unity is a volume fraction vector. A volume integrated parameter placed in the expression can then be divided by the volume fraction vector to yield its volume averaged vector. This approach is used for both axial and angular discretizations, as well as surface and volume integrated parameters.

2.2 Thermal-Structural Models

Thermomechanical models include geometries of the target pin encapsulating housing and its internal components, including the 52 NpO_2/Al pellet stack. A 2-D R-Z model, previously developed for the production target design, includes the entire target pin and all internal components. The 3-D model includes only two localized pellets and the adjacent cladding. This model is meant only to conservatively capture 3-D effects including the asymmetric bulk temperature.

2.2.1 Gap & Contact Conductance

As described in previous development work [7], centerline pellet temperatures are driven by the heat transfer in the pellet/clad gap. The basic equation for gap conduction, h, is shown in Eq. 5 below, where it is the sum of the gas gap and solid-spot/contact conductance. The gas gap term includes a thermal conductivity, k_g, reduction due to fission gases, FGR_f, the gap size itself, δ (calculated by contact pairs in the solid mechanics interface), and "thermal jump" terms, g_i, that account for ineffective gas-to-solid heat transfer at each surface.

$$h = \frac{FGR_f k_g}{\delta + g_1 + g_2} + h_s \quad \textbf{(5)}$$

The thermal jump is a factor of gas properties (including the accommodation coefficient, mean free path, viscosity, etc.) [9]. Thermal jump for a gas mixture can be calculated as a weighted average of the mass fractions. The contact conductance is driven by the contact pair pressure (if present) and may be defined for elastic or plastic deformation, or interpolated using a plasticity index, ψ, as shown in Eq. 6.

$$h_s(\psi) = \begin{cases} \psi < 0.7 & h_e = 1.55\left({k_m m}/{\sigma}\right)\left(P\sqrt{2}/{E' m}\right)^{0.94} \\ 1.0 > \psi > 0.7 & \frac{1.0-\psi}{0.3}(h_p - h_e) \\ \psi > 1.0 & h_p = 1.13\left({k_m m}/{\sigma}\right)\left(P/H\right)^{0.94} \end{cases} \quad \textbf{(6)}$$

2.3 Transient Model

The accident transient model consists of a pipe flow model of the target holder flow paths for seven individual pins, which consists of 1-D pipes to represent flow paths in 3-D space. In addition, two 3-D target cladding geometries are present to represent the hottest pin (pin 1) and an averaged pin cladding. Non-isothermal pipe flow physics are solved on the pipe flow domain and heat transfer in solids is solved in the cladding domains.

2.3.1 Integration Operators

Integration operators are used to create a two-way coupling between the pipe flow components and housing/cladding: (1) Linear heat rates are mapped from the cladding to the pipe flow channels, and (2) The bulk temperature is mapped from the pipe flow channels to the cladding. Both are calculated as a function of channel position.

This is accomplished using an antiderivative approximation within the integral coupling operators. By using logical expressions and the *dest* operator, as shown in Eq. 7, an integral operator can be used to approximate an antiderivative.

$$\int_a^x u(x')dx' = \int_a^b u(x')[x' \le dest(x)]dx' \quad \textbf{(7)}$$

Using the bulk temperature as an example, the volume-averaged antiderivative of the temperature, T, along a channel of cross-section A_{xy} from channel position a to z is described in the first part of Eq. 8 as it approaches position a. This is simplified using L'Hôpital's rule as the ratio of derivatives to the bulk temperature at position a.

$$\lim_{z\to a} \frac{\iiint_a^z T(x',y',z')dx'dy'dz'}{A_{xy}(z-a)} = \frac{\frac{d}{dz}\iiint_a^z T(x',y',z')dx'dy'dz'}{\frac{d}{dz}A_{xy}(z-a)} = \frac{\iint_{\Omega_{xy}} T(x',y',z)dx'dy'}{A_{xy}} = T_b(a) \quad \textbf{(8)}$$

At position b in a channel of length a to b, the solution to Eq. 8 would be the average channel temperature. The antiderivative from position z to b could then be simplified similarly to solve to the bulk temperature at position b and the average temperature at position a.

Combining these two approximations with adjusted z coordinates gives a continuous approximation of the bulk temperature.

This approximation is therefore most accurate for properties driven by inputs symmetric about the horizontal midplane. In the case of the bulk temperature, the targets are placed at the horizontal midplane of the reactor and thus the heat flux is symmetric. Eq. 8 also assumes that the cross-sectional area does not have a high gradient with respect to channel position (true for the targed finned region).

2.4 Boundary & Initial Conditions

Boundary conditions and initial values for the models presented above are discussed here.

For the thermal hydraulic models, the outlet pressure is set by reactor design or flow test. The inlet flow is set to the flow test or adjusted to yield the ~100 psi pressure drop across the experiment positions. Wall functions are solved at target and holder surfaces, while symmetry is set along the sector interfaces. Initial values are set to the inlet velocity, and outlet pressure, unless a solution is used from a previous study step. Wall heat fluxes are taken from the thermal-structural model solutions.

In the thermal-structural models, the geometry is constrained at the axial centerline and target bottom. Thermal insulation is also specified at the target top and bottom, and convective cooling, with a modified heat transfer coefficient to include a calculated oxide layer, is defined at the target outer surface.

In the transient model, the time-dependent boundary conditions are taken from the HFIR plant model for the two accidents analyzed. A steady-state solution is solved for the initial condition.

3. Results of Simulations

The PARDISO direct solver is used for the thermal-structural simulations, while the MUMPS direct solver is used for thermal hydraulic simulations in order to utilize distributed parallel processing. One compute node containing 48 cores on two processors with 512 GB RAM is utilized for the transient and thermal-structural studies while 1-2 of these compute nodes are used for the thermal-hydraulic studies.

For the thermal hydraulic simulations, a coarse, normal, and fine mesh are solved with 2-8 boundary layers and a stretching factor between 1.4 and 1.1. Free tetrahedral mesh are used in the more complex geometric features, and swept mesh is used for the remaining features. Approximately 1.3 – 4.4 million mesh elements are used to discretize the geometry and 1 - 4 million degrees of freedom (DOF) are solved.

The flow test model is first solved, with the detailed inlet pressure drop and flow shown in Fig. 4. Good comparison is observed between the experimental results (measured in terms of pressure drop vs. volumetric flow) as shown for the bulk pressure drop to the right of Fig. 4.

Two design-aid parameters of interest are (1) to identify the connecting slot location and size necessary to allow sufficient flow the central target channel, and (2) ensure that the total target holder flow remain at ~5 gpm per target pin. The sufficient connecting slot is identified and confirmed via the flow test. The final design differs slightly from the flow test, however, in the outlet region, as shown in Fig. 5. One outlet flow path is opened in the target cup due to a higher seated position in the final design target. To compensate, a reduced holder orifice diameter is calculated to yield the desired flow rates.

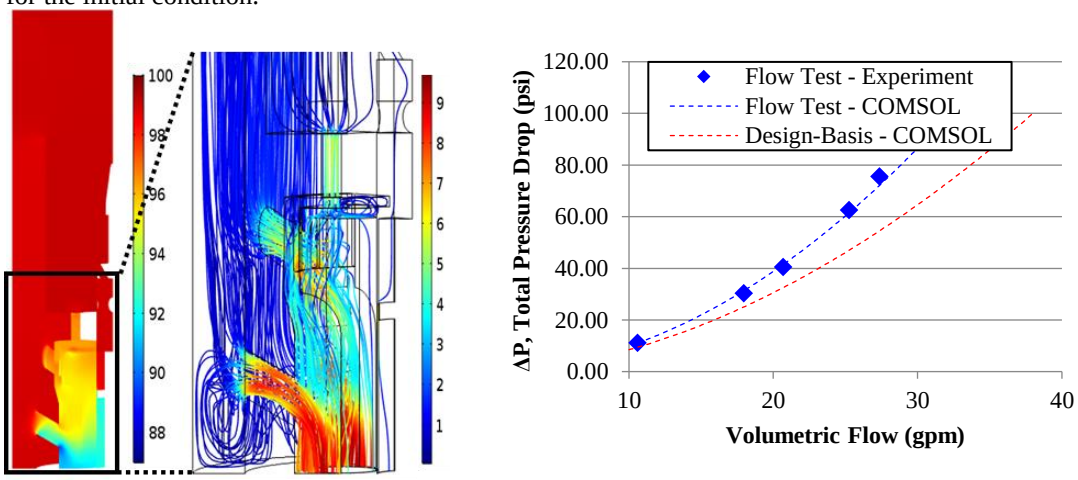

Figure 4. The inlet flow region (left, psi and m/s) and flow validation (right).

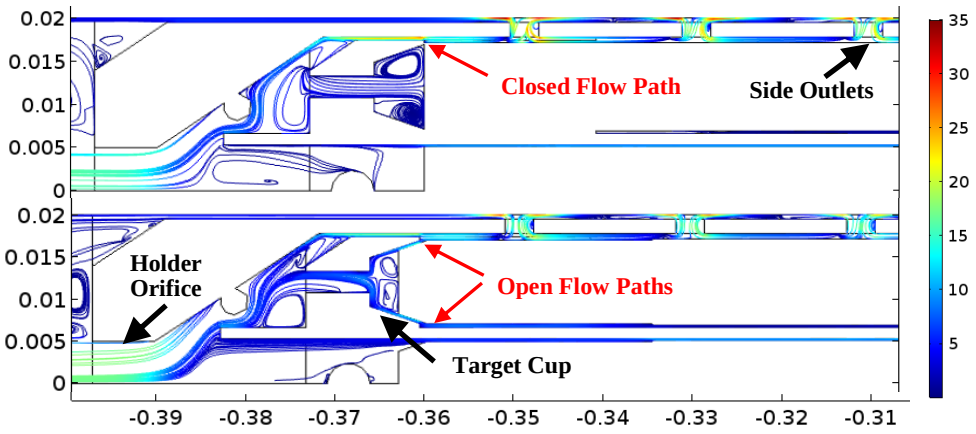

Figure 5. Z-X streamlines with velocity color profile (m/s) of the flow test (top) and design (bottom) outlet regions.

For the safety assessments, four eccentric positions were chosen, at varying rotations and for both the central (pin 7) and peripheral target pin (pin 1). The fourth eccentric position for the peripheral target pin 1 is identified as the limiting case with respect to surface burnout margin, as shown in Fig. 6.

The 2-D R-Z target pin model is assessed at the end-of-cycle (EOC)-1, 2, and 3 for pins 1 and 7, where pin 1 results are found to be more limiting, despite the near factor of 2 reduction in flow to the central channel pin.

The pellet stack centerline temperatures, where the temperature gradient in the pellet/clad gap is predominant, are driven by the gap size and contact pressure. This gap size is largely affected by the swelling and densification curves of the pellets obtained by post-irradiation examination. There is an initial densification or volume reduction, due to radiation sintering, followed by recovery due to swelling and subsequent net volume increase. The maximum pellet centerline temperature occurs at EOC-1 while the maximum stress/strains occur at EOC-3.

This neutron irradiation-driven effect on the pellet stack temperature profiles is illustrated in Fig. 7, which shows the best-estimate pellet stack temperature profiles for the 2-D R-Z target pin at EOC-1, 2, and 3. The maximum temperature in the pellet stack shifts from the horizontal midplane to the pellet stack ends due to the time-dependent densification/swelling which has its minima at changing locations within the pellet stack.

The 3-D pellet/clad model utilizes the asymmetric convective cooling inputs, due to asymmetric channels and eccentricity, calculated in the limiting eccentric thermal hydraulic calculations. Pin 1 is assessed at thermally and structurally limiting conditions at EOC-1 and -3, respectively, at the limiting pellet positions determined in the 2-D R-Z model results. The results, solving 1-2 million DOF, identify a slight, non-consequential decrease in safety margin for the 3-D results.

The transient model is solved for two thermally limiting HFIR accident transients: the small break loss-of-coolant accident (SBLOCA) and the loss of offsite power (LOOP). Transients were computed over their observed limiting conditions (a few minutes), using multiple time-stepping schemes (free BDF and generalized-α) and solving ~ 0.3 million DOF. The simulation results showed no surface burnout or pellet melting under either transient, where the SBLOCA (the more limiting transient) burnout margin is shown in Fig. 8.

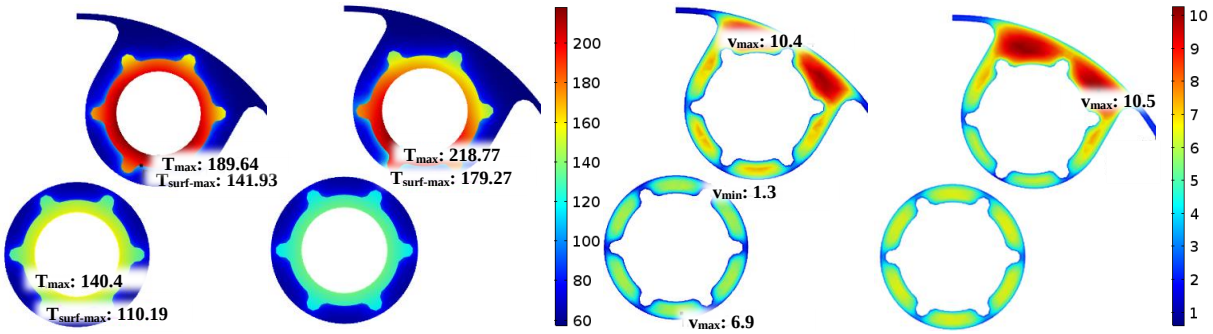

Figure 6. X-Y cross-section of temperatures (left, °C) and flow velocities (right, m/s) for the nominal and 4th eccentric case.

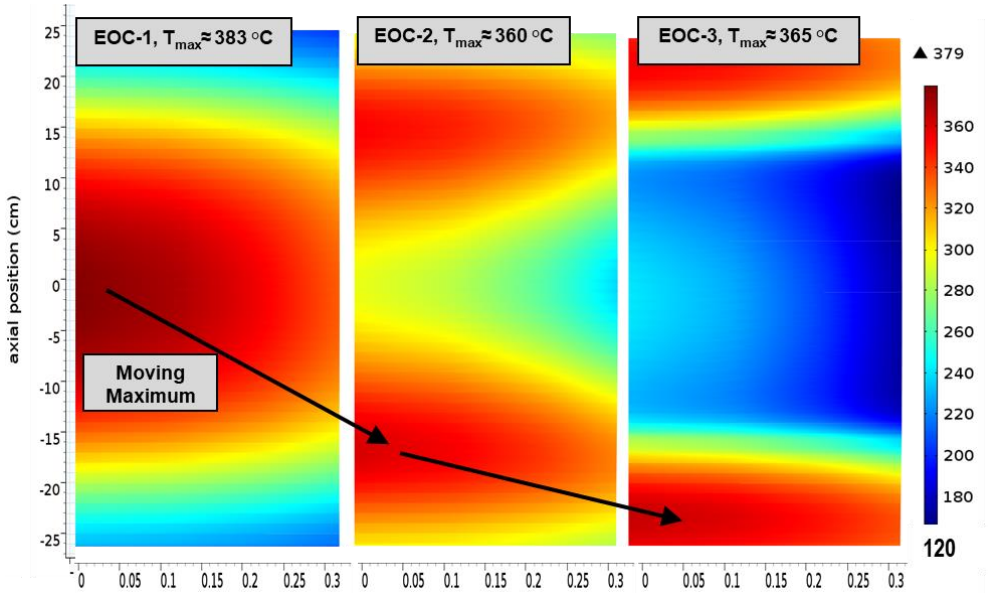

Figure 7. 2-D R-Z pellet stack temperature profiles (°C) at EOC-1, 2, and 3 (dimensions in cm).

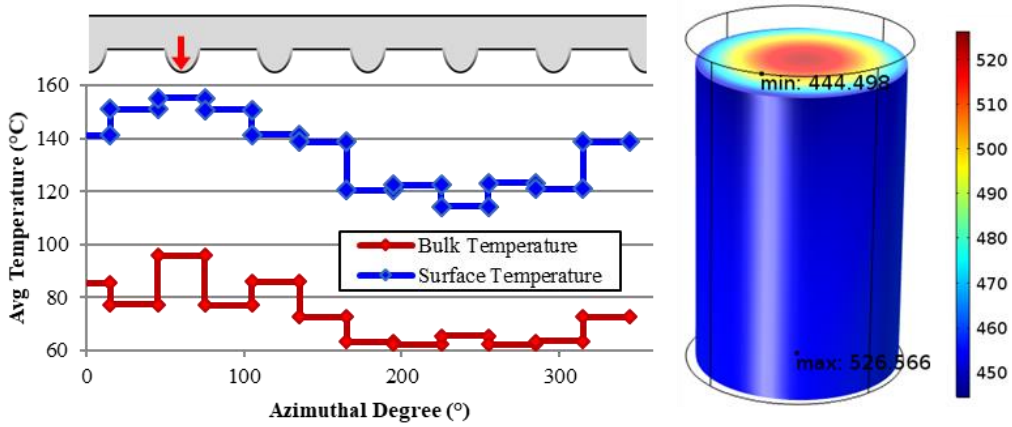

Figure 8. Asymmetric convective cooling inputs (left) and 3-D pellet temperature profile (right, °C).

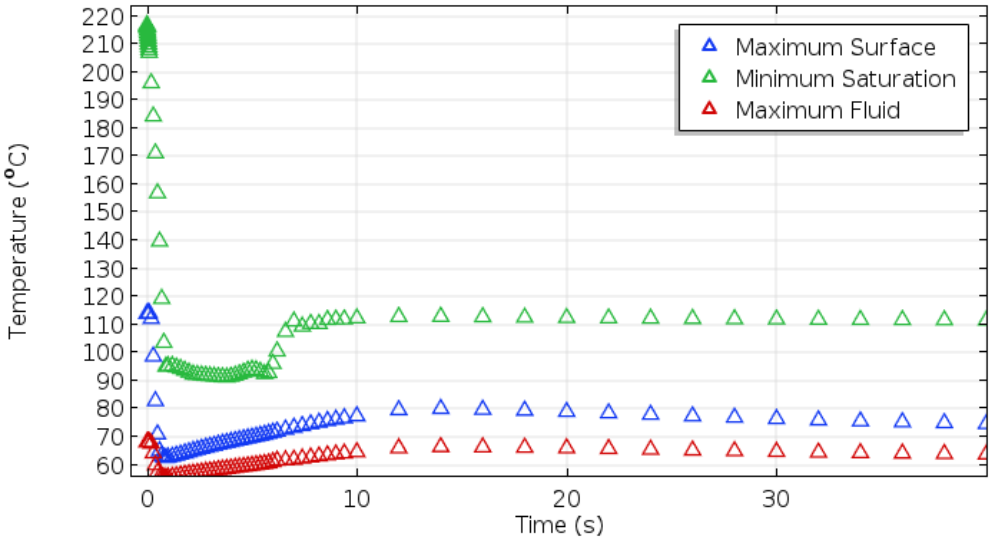

Figure 9. Minimum saturation and maximum target/coolant temperatures for the SBLOCA transient.

4. Conclusions

A detailed series of models is developed in order to adequately encompass the required safety basis for an updated and more complex 2nd Generation target holder design. Thermal-hydraulic simulations identified flow path characteristics for design-aid while addressing potential asymmetric flow positions and their safety impact. The detailed 2-D R-Z thermal-structural methodology formerly developed was updated, and a 3-D model captured asymmetric effects. Finally, a transient model coupling 1-D flow components and 3-D heat structures addressed HFIR accident transients.

The CFD models developed in this work did not consider fluid-structure interaction or include a moving mesh, which may be incorporated later, if deemed necessary. A complete 3-D model combining the non-linear effects at the pellet/housing interface with the computational demand of CFD would most likely require a well-defined solution approach using iterative solvers with domain decomposition, would require a well-defined answer for stable convergence.

Future work will likely include a tighter coupling of thermal-hydraulic and thermal-structural models, in order to more accurately assess safety margin. Increased safety margin from improved methodology can aid in updated target designs including allowance of increased neptunium loading to raise ^{238}Pu throughput.

5. References

[1] Hurt, C.J., Freels, J.D., et. al., Thermo-mechanical Safety Analyses of Production Design Experiments for 238Pu Production, ASME Journal of Nuclear Engineering and Radiation Science, NERS-16-1069 (2018).

[2] Hurt, C.J., Deterministic Neutron Transport and Multiphysics Experimental Safety Analyses at the High Flux Isotope Reactor, PhD dissertation, University of Tennessee (2016).

[3] COMSOL Multiphysics® v. 5.2 and v. 5.3, www.comsol.com, COMSOL AB, Stockholm, Sweden, 2015 and 2017.

[4] Howard, R., The Evolution of HFIR Cermet Pu-238 Production Targets, ANS NETS 2018 – Nuclear and Emerging Technologies for Space, Las Vegas, NV (2018).

[5] Hobbs, R.W., Chandler, D., Hurt, C.J., et. al., "Potential Improvements to 238Pu Production Targets for the High Flux Isotope Reactor," ANS Winter Meeting 2015, Washington, DC (2015).

[6] Chandler, D., Ellis, R.J., Development of an Efficient Approach to Perform Neutronics Simulations for Plutonium-238 Production, PHYSOR 2016, Sun Valley, Idaho (2016).

[7] Hurt, C.J., Freels, J.D., et. al., Thermal Safety Analyses for the Production of Plutonium-238 at the High Flux Isotope Reactor, ORNL/TM-2016/234, Oak Ridge National Laboratory (2016).

[8] Reference Fluid Thermodynamic and Transport Properties (REFPROP), NIST Standard Reference Database, Version 9.11, Copyright 2013 by U.S. Secretary of Commerce (2014).

[9] Madhusudana, C.V., Thermal Contact Conductance, Springer-Verlag, New York, NY (1995).

6. Acknowledgements

The studies documented in this paper were conducted by the Research Reactors Division at ORNL. The authors would like to thank ORNL staff and the COMSOL technical support staff for their advice during the development of the models described in this paper. The author would also like to thank Valerie Fudurich of ORNL for her technical review of this paper.